

**Electronic bound states in the continuum above (Ga,In)(As,N)/(Al,Ga)As quantum wells**Asaf Albo,<sup>1,\*</sup> Dan Fekete,<sup>2</sup> and Gad Bahir<sup>1</sup><sup>1</sup>*Department of Electrical Engineering, Technion-Israel Institute of Technology, Haifa 32000, Israel*<sup>2</sup>*Department of Physics, Technion-Israel Institute of Technology, Haifa 32000, Israel*

(Received 5 June 2010; revised manuscript received 21 October 2011; published 14 March 2012)

Using intersubband photocurrent spectroscopy, we have demonstrated that a bound state in the continuum exists above (Ga,In)(As,N)/(Al,Ga)As quantum wells. The photocurrent spectrum and responsivity show that the excited-state energies lie far above the potential barrier of the quantum well, and the bound nature of the states was confirmed from the long lifetime of the excited carriers and a small coupling with the surrounding continuum. Applying optical phonon scattering theory, we have demonstrated that the relaxation process is governed by scattering from localized nitrogen states to the three-dimensional continuum.

DOI: [10.1103/PhysRevB.85.115307](https://doi.org/10.1103/PhysRevB.85.115307)

PACS number(s): 73.22.-f, 68.65.Fg, 71.20.Nr

**I. INTRODUCTION**

The concept of bound states in the continuum (BSICs) was proposed by von Neumann and Wigner shortly after the birth of quantum mechanics.<sup>1</sup> BSICs are spatially confined states with infinite lifetime that have an energy lying above the potential barrier and are embedded in the higher-energy continuum. The potentials and conditions that support BSICs have been widely studied in the literature (e.g., see Ref. 2). BSICs can result from interaction between quasistationary (resonance) states in special potentials, which provides resonances with practically infinite lifetimes.<sup>3,4</sup> About three decades ago, the use of superlattices to construct potentials that can support BSICs was proposed by Herrick<sup>5</sup> and Stillinger.<sup>6</sup> However, it was only in 1992 that Capasso *et al.* observed the existence of an electronic bound state with energy far above the barrier height of the potential quantum well (QW) in superlattice structures.<sup>7</sup> Similar superlattice structures, but with states confined in the barrier, had been demonstrated before this by Salzman *et al.*<sup>8</sup> Bastard *et al.*<sup>9</sup> conducted earlier work on virtual quasibound states in a continuum arising from constructive interference.

The bound states demonstrated so far, both experimentally and theoretically, were formed because of unique potential symmetries. For example, in Capasso *et al.*'s work, the superlattice was designed so that the Bragg reflection spatially localized the states corresponding to the first continuum resonance of a QW. The energy of the bound state could be understood as being of a deep level in the superlattice bandgap, arising from the introduction of an artificial defect in a periodic superlattice structure.

In a recent work by Plotnik *et al.*,<sup>10</sup> the issue of BSICs was addressed again, first by defining the BSIC characteristics following by reviewing approaches to implement and observe BSICs experimentally. As concluded by these authors, BSICs have never been observed in any system—quantum or classical. Under the assumption that the concept of BSICs is based on interference and not restricted to quantum systems; the authors presented an experimental observation of BSICs that carried out in a two-dimensional optical waveguide array structure in which the bound state is decoupled from the continuum by virtue of symmetry only.

In this work, we demonstrate experimentally that the combination of an N-doped (Ga,In)As and a quantum confinement

is the origin of three-dimensional (3D) localized, both spatially and energetically, bound state that is in resonance with a 3D delocalized continuum of states. This BSIC is decoupled from the continuum by an anticrossing interaction, taking place between the original resonance N states and the above-barrier continuum.

The III–V–N (diluted nitrides) semiconductor compounds have attracted growing interest over the past few years because of their unique electronic properties. Well-known features are the large bowing of the band gap observed in many III–V–N semiconductors, an increase in the electron effective mass, and a reduced temperature dependence of the band gap energy.<sup>11</sup> A major breakthrough in the interpretation of experimental results was achieved with the demonstration by Shan *et al.*<sup>12</sup> that the reduction in the energy gap arises from a band anticrossing (BAC) interaction between the conduction band edge  $E_C$  of the III–V host and a higher-lying band  $E_N$  composed of localized nitrogen resonant states. This interaction can be treated as a perturbation, which leads to an eigenvalue problem. Solving the eigenvalue problem gives two subband energies: a fundamental new band gap  $E_-$  and a higher new extra band  $E_+$ . The valence band is virtually unaffected. The BAC model is consistent with a range of experimental data and accurately reproduces the observed dependence of the band gap of Ga(As,N) and (Ga,In)(As,N) on the N content. Despite the wide success of the two-level BAC model, it fails to explain several sets of experimental data.<sup>13</sup>

Theoretical studies based on the tight-binding method<sup>14</sup> and pseudopotential supercell calculations of the band gap that take into account N cluster states<sup>15</sup> generally support the BAC model, at least regarding the conduction band minimum. In addition, the theoretical basis for using the BAC model was established from tight-binding calculations and can be extended to the 10-band  $k$ - $p$  model.<sup>14</sup> So far, to the best of our knowledge, there have been few publications on  $E_-$  to  $E_+$  transitions, and no information is available on the carrier dynamics of these transitions.

In this work, we demonstrate experimentally using intersubband (ISB) photocurrent (PC) spectroscopy the existence of bound states in the continuum above (Ga,In)(As,N)/(Al,Ga)As QW barriers. We assigned the PC to transitions from a confined  $E_-$  level in the QWs to a localized resonant  $E_+$  level in the continuum. The experimental results of the PC spectroscopy

are analyzed using both the BAC model and its extension to 10-band  $k \cdot p$  model calculations. Our analysis relies on the unique nature of the  $E_-$  and  $E_+$  dispersion curves, as discussed later.

The paper is organized as follows. In Sec. II, the sample structures and experimental setup are introduced. In Sec. III, the 10-band  $k \cdot p$  model calculations on the bulk and QW electronic structures are described. This model was applied to interpret the experimental ISB PC spectra, focusing on the relationships between the QW and the barrier composition, dimensions, and transition energies. The experimental results are presented in Sec. IV. Finally, the PC, dark current, and excited electron dynamics are analyzed based on calculations of the coupling between the excited bound state and the continuum and on longitudinal optical (LO) phonon scattering theory using the  $E_-$  and  $E_+$  dispersion curves.

## II. SAMPLE STRUCTURES

The samples were grown using the metal organic chemical vapor deposition technique on semi-insulating (001)-oriented (Ga,As) substrates, using trimethylgallium, trimethylindium, arsine, and dimethylhydrazine as the material sources and dimethyl telluride as the N-type doping source. Multiquantum well (MQW) (Ga,In)(As,N)/(Ga,As) and (Ga,In)(As,N)/(Al,Ga)As structures with 10 periods of Te-doped (nominal doping level of  $2 \times 10^{17} \text{ cm}^{-3}$ ) 25-Å  $\text{Ga}_{0.75}\text{In}_{0.25}\text{As}_{0.98}\text{N}_{0.02}$  QWs and 480-Å undoped GaAs—or 390-Å  $\text{Al}_{0.26}\text{Ga}_{0.74}\text{As}$ —barriers were grown as the active region of a quantum well infrared photodetector (QWIP). The MQW structure was sandwiched between 5000-Å-thick, highly Te, N-doped ( $2 \times 10^{19} \text{ cm}^{-3}$ ) (Ga,As) contact layers. The doped active (Ga,In)(As,N) QWs were grown at 500 °C. The low growth temperature was necessary for the incorporation of 1%–2% N into  $\text{Ga}_{0.75}\text{In}_{0.25}\text{As}$  (see page 15 in Chapter 2 in Ref. 11). The undoped (Ga,As) and (Al,Ga)As barrier layers were grown at 750 °C. A reference  $\text{Ga}_{0.75}\text{In}_{0.25}\text{As}/\text{Al}_{0.26}\text{Ga}_{0.74}\text{As}$  QWIP structure without any nitrogen was grown using the same growth conditions with an identical structure to the (Ga,In)(As,N) QWIP. The dilute nitride growth conditions are not optimal for (Ga,In)As QWs. Standard photolithography and wet etching techniques were used to form  $200 \times 200 \mu\text{m}^2$  mesa structures. N-type ohmic contacts were formed using Ni–Ge–Au–Ni–Au alloy deposited onto the top and bottom contact layers and annealed at 400 °C.

High-resolution x-ray diffraction, low-temperature photoluminescence (PL), time-of-flight secondary ion mass spectroscopy, and transmission electron microscopy were employed to characterize the quality of the MQW structures.<sup>16–18</sup> The QWIP substrates were polished at an angle of 45° to enable irradiation at both the S and the P polarizations, allowing an analysis of polarization effects on the ISB transitions. In the PC measurements, the samples were illuminated using an infrared light incident normal to the 45° polished facet. The PC was measured using a Fourier transform infrared spectrometer (Bruker-Equinox 55) employing internal near-infrared (NIR) and midinfrared sources.

In the PC measurements, the detector was mounted in a closed-cycle helium flow optical cryostat and characterized using different applied bias voltages with a chopper frequency

of  $f = 135 \text{ Hz}$ . All measurements were conducted using a 1.18- $\mu\text{m}$  high-pass filter to prevent any “parasitic” response related to the (Ga,As) contact layers and interband PC. The temperature-dependent photoresponse spectra of the QWIP structures were obtained using different bias voltages. The dark current was measured using a standard semiconductor parameter analyzer over the relevant operating voltage span at several temperatures.

Transmission measurements were conducted in the front-illumination (normal incident) mode with respect to a reference (Ga,As) substrate using a standard PerkinElmer ultraviolet-visible NIR spectrometer. The intraband PC responsivity was measured using a calibrated 2-mW, 1.55- $\mu\text{m}$  semiconductor laser light illumination source oriented normal to the polished facet.

## III. ELECTRONIC BAND STRUCTURE CALCULATIONS

We now describe the electronic structure modeling of the synthesized structures described previously. The band structure, wave function, and ISB transition energies of symmetrical (Ga,In)(As,N)/(Al,Ga)As QWs were calculated using a 10-band  $k \cdot p$  model that assured an accurate description of the effect of localized nitrogen resonant-level coupling to the extended conduction and valence band states.<sup>19</sup> The model used was a finite difference procedure that took into account the strain. The binary compounds and the (Ga,In)(As,N) nitrogen parameters (i.e., the localized nitrogen-related energy-level position  $E_N$  and the interaction strength of  $E_N$  with the conduction band states  $V_{NC}$  and valence band states  $P_N$ ) were taken from Ref. 17 and references therein. The two samples used had structures designed to have  $E_N$  levels lying above the QW barrier edge so that they would anticross with the 3D continuum states.

Figure 1(a) shows the results of calculations obtained at room temperature (RT) that demonstrate the restructured  $E_-$  and  $E_+$  subband dispersion curves resulting from BAC interactions between the  $E_N$  and the extended states of the conduction band in a strained layer of  $\text{Ga}_{0.75}\text{In}_{0.25}\text{As}_{0.98}\text{N}_{0.02}$  on GaAs. The valence band edge of (Ga,As) before spin-orbit split-off and strain effects was chosen as the energy reference level in our model.

Figure 1(b) shows the energy levels of the first two bound levels in the conduction band of the  $\text{Ga}_{0.75}\text{In}_{0.25}\text{As}_{0.98}\text{N}_{0.02}/\text{GaAs}$  QW,  $E_{1-}$  and  $E_{2-}$ , where  $E_{2-} - E_{1-} \approx 180 \text{ meV}$ . The (Ga,In)(As,N)  $E_+$  level [Fig. 1(a)] becomes the  $E_{1+}$  and  $E_{2+}$  resonant levels in the continuum of the heterostructure, where  $E_{2+} - E_{1+} \approx 4 \text{ meV}$ , and is shown by the single dashed-dotted line (marked  $E_{1+,2+}$ ) in Fig. 1(b). The replacement of the GaAs barrier by  $\text{Al}_{0.26}\text{Ga}_{0.74}\text{As}$  had a very small effect on  $E_{1-}$  and  $E_{2-}$  ( $\sim 20 \text{ meV}$ , as shown in Fig. 1(b)), which is less than the experimental accuracy. In addition, this barrier replacement had a negligible effect on  $E_{1+,2+}$ , because these levels in the continuum depend on the N content in the (Ga,In)(As,N) layer, which was the same in the two QWs. Figure 1(c) shows the dispersion in the  $xy$  plane of the (Ga,In)(As,N)/(Ga,As) QW. The RT calculated value for  $E_{1-}$  to  $HH_1$  interband transition energy was 1.0358 eV, which agrees well with the PL experimental data of 1.03 eV reported elsewhere.<sup>17</sup>

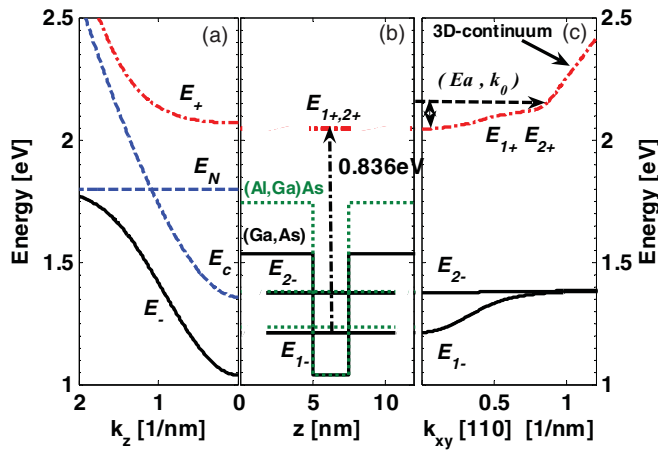


FIG. 1. (Color online) (a) Calculations with the 10-band  $k$ - $p$  model of the energy band dispersion curves of a  $\text{Ga}_{0.75}\text{In}_{0.25}\text{As}_{0.98}\text{N}_{0.02}$  on GaAs coherently grown bulk layer.  $E_N$  and  $E_C$  (dashed blue lines) are the energies of the original states, and  $E_-$  and  $E_+$  (solid black and dashed-dotted red lines, respectively) are the energies of the newly formed states. (b) Energy subband levels in a 25-Å  $\text{Ga}_{0.75}\text{In}_{0.25}\text{As}_{0.98}\text{N}_{0.02}$  QW with GaAs (solid black) and  $\text{Al}_{0.26}\text{Ga}_{0.74}\text{As}$  (dotted green) barriers. (c) The  $\text{Ga}_{0.75}\text{In}_{0.25}\text{As}_{0.98}\text{N}_{0.02}/\text{GaAs}$  QW's energy subband dispersion in the [110] direction in the QW plane. The valence band edge of (Ga,As) before spin-orbit split-off and strain effects was chosen as the energy reference point in our model.

IV. EXPERIMENTAL RESULTS

The PC spectra of the two QWIP structures as a function of temperature from 150 to 300 K are shown in Fig. 2(a) and 2(c). The transmission spectrum of normal incident illumination on the (Ga,In)(As,N)/(Ga,As) structure is shown in Fig. 3(a), and the dark current at 300 K of the two QWIP structures is shown in Fig. 3(b). The PC spectra, front illumination transmission

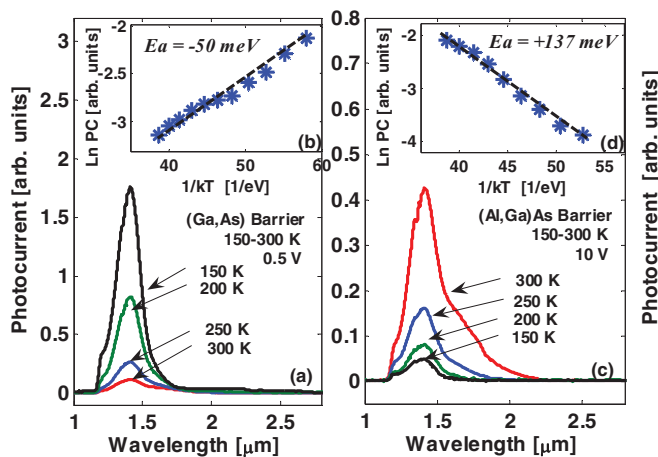


FIG. 2. (Color online) (a) PC spectral response of a  $\text{Ga}_{0.75}\text{In}_{0.25}\text{As}_{0.98}\text{N}_{0.02}/\text{GaAs}$  QWIP at various temperatures (150–300 K) under a bias of 0.5 V (Ref. 17). (b) PC vs  $1/kT$  for a  $\text{Ga}_{0.75}\text{In}_{0.25}\text{As}_{0.98}\text{N}_{0.02}/\text{GaAs}$  QWIP. (c) PC spectral response of a  $\text{Ga}_{0.75}\text{In}_{0.25}\text{As}_{0.98}\text{N}_{0.02}/\text{Al}_{0.26}\text{Ga}_{0.74}\text{As}$  QWIP at various temperatures (150–300 K) under a bias of 10 V. (d) PC vs  $1/kT$  for a  $\text{Ga}_{0.75}\text{In}_{0.25}\text{As}_{0.98}\text{N}_{0.02}/\text{Al}_{0.26}\text{Ga}_{0.74}\text{As}$  QWIP.

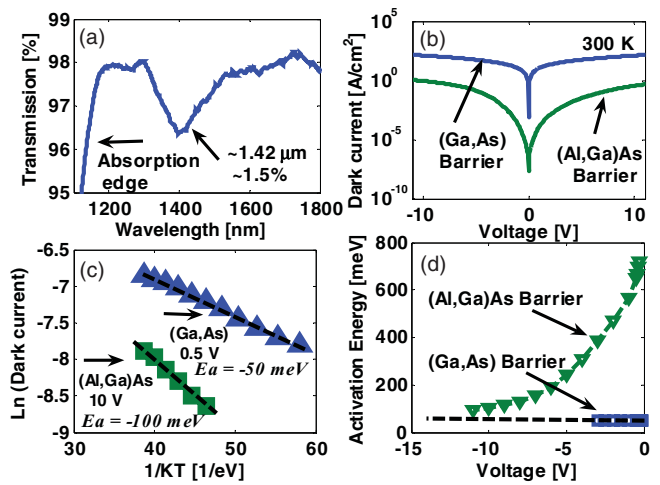


FIG. 3. (Color online) (a) Front illumination transmission measurements of a  $\text{Ga}_{0.75}\text{In}_{0.25}\text{As}_{0.98}\text{N}_{0.02}/\text{GaAs}$  QWIP. (b) Dark current vs bias at RT. (c) Dark current vs  $1/kT$  for the  $\text{Ga}_{0.75}\text{In}_{0.25}\text{As}_{0.98}\text{N}_{0.02}/\text{GaAs}$  and  $\text{Ga}_{0.75}\text{In}_{0.25}\text{As}_{0.98}\text{N}_{0.02}/\text{Al}_{0.26}\text{Ga}_{0.74}\text{As}$  QWIP structures. (d) Dependence of the absolute value of the activation energy on the bias voltage extracted from the dark current measurements as a function of temperature for both (Ga,In)(As,N)/(Ga,As) and (Ga,In)(As,N)/(Al,Ga)As QWIP structures.

spectrum, and dark current characteristics in Figs. 2–4 show several interesting and unique features:

- (1) The dominant PC signals of the two QWIP structures showed a maximum occurring at  $\sim 1.42 \mu\text{m}$  (870 meV), indicating that the transition energy involved was independent of the barrier height and was to an upper level that was higher than the barrier of both structures:  $\sim 500$  and  $700$  meV for the (Ga,As) and (Al,Ga)As barriers, respectively.
- (2) The two PC peaks were nearly polarization independent, as demonstrated for a (Ga,In)(As,N)/(Ga,As) QWIP.<sup>17</sup> A clear (Ga,In)(As,N) absorption edge and deep ISB

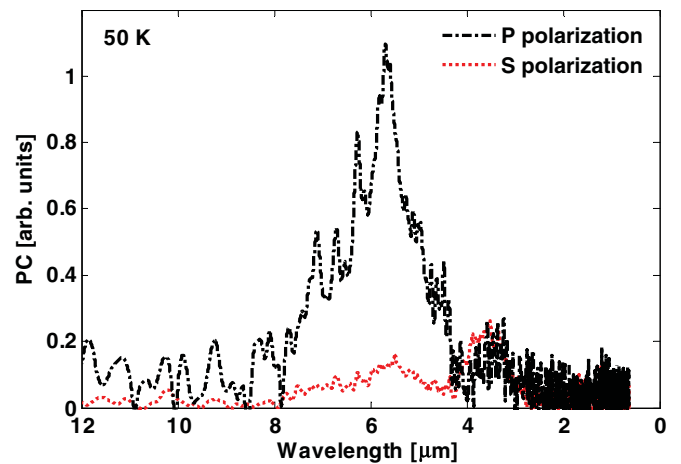


FIG. 4. (Color online) PC spectral response of the  $\text{Ga}_{0.75}\text{In}_{0.25}\text{As}/\text{Al}_{0.26}\text{Ga}_{0.74}\text{As}$  QWIP reference structure measured at 50 K in the wedge illumination under bias of 0.2 V and under P polarization (black dashed-dotted line) or S polarization (red dotted line).

absorption located at longer wavelengths of  $\sim 1.42 \mu\text{m}$  were observed in the front illumination transmission spectrum of the (Ga,In)(As,N)/(Ga,As) MQW sample shown in Fig. 3(a). Because normal incident illumination enables only S polarized (Transverse-Electric; TE) absorption, this is an additional confirmation of the measured polarization-independent PC response.

(3) Figure 4 shows the ISB PC spectra at 50 K of the reference (Ga,In)As/(Al,Ga)As QWIP structure in the wedge illumination configuration. As expected for a conventional III-V MQW, the PC signal was completely P polarized and the ISB PC peak was observed at  $\sim 6 \mu\text{m}$  because of the shallower (Ga,In)As/(Al,Ga)As QW. The characteristic PC peak occurring at  $1.42 \mu\text{m}$  [Fig. 2(a) and 2(c)] was absent in the reference sample that has zero nitrogen content.

The PC measurements of the two nitrogen containing QWIPs were taken using different bias voltages of 0.5 and 10 V for the (Ga,As) and (Al,Ga)As QWIPs, respectively. The reason for the different bias voltages was the need to reach a similar quasi-Fermi energy level in the two QWIPs, which had, at zero or low bias, different free carrier concentrations in the QWs because of the absence of barriers between the highly doped (Ga,As) contact layers and the wells in the (Ga,In)(As,N)/(Ga,As) QWIP.

(4) The dark current behavior with temperature showed a pure thermionic emission behavior for both structures in the temperature range used in this work and the relevant operating voltages. The activation energies of the dark currents as a function of bias are shown in Fig. 3(c) and 3(d). We extracted the quasi-Fermi energy-level position from the activation energies using the expression  $I_d \propto \exp(-(E_{Cb} - E_F)/kT)$ , where  $E_{Cb}$  is the barrier conduction band edge. As shown in Fig. 3(d), for a bias of 10 V on the (Al,Ga)As QWIP, the absolute value of the dark current activation energy was  $\sim 100 \text{ meV}$  and the position of the quasi-Fermi energy lay far above the  $E_{2-}$  energy level [Fig. 1(b)], about the same as in the (Ga,As) barrier QWIP at 0.5 V. As expected, because of the difference in barrier heights, the dark current for the (Ga,In)(As,N)/(Al,Ga)As QWIP was four to six orders of magnitude lower than the dark current of the (Ga,In)(As,N)/(Ga,As) QWIP, as shown in Fig. 3(b).

(5) Surprisingly, an opposite experimental temperature dependence was observed for the two QWIP PC signals, as shown in Fig. 2(a) and 2(c). The PC signal for the (Ga,In)(As,N)/(Ga,As) QWIP decreased, and the PC signal for the (Ga,In)(As,N)/(Al,Ga)As QWIP increased with increasing temperature. The activation energy of the PC signal extracted from the Arrhenius plots shown in Fig. 2(b) and 2(d) was negative ( $-50 \text{ meV}$ ) and positive ( $+137 \text{ meV}$ ) for the (Ga,In)(As,N)/(Ga,As) and (Ga,In)(As,N)/(Al,Ga)As QWIPs, respectively.

(6) The PC dependence on the bias (electric field from 5 to 20 keV/cm), shown in Fig. 5, was linear for the (Ga,In)(As,N)/(Ga,As) QWIP structure (on keeping the bias in the range at which the quasi-Fermi energy was constant, as shown in Fig. 3(d)). For the (Al,Ga)As QWIP, the PC dependence on the bias was nonlinear because of the strong dependence of the carrier density in the QWs on the bias, as discussed previously.

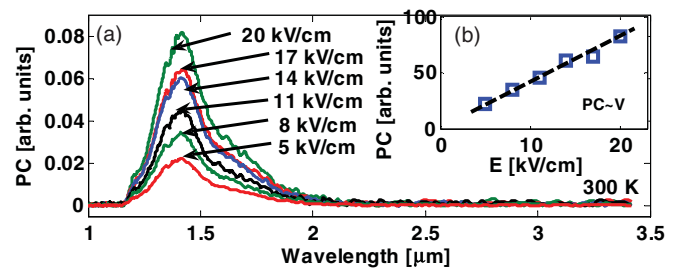


FIG. 5. (Color online) (a) PC spectra of a  $\text{Ga}_{0.75}\text{In}_{0.25}\text{As}_{0.98}\text{N}_{0.02}/\text{GaAs}$  sample with different applied electric fields at RT. (b) PC intensity as function of the electric field.

(7) The relative PC width at half maximum,  $\Delta\lambda/\lambda_{\text{peak}} \approx 14\%$ , was narrow, indicating bound to quasibound transition characteristics.<sup>20</sup>

(8) The responsivity and gain were very high compared with standard QWIPs, in the range at which  $R \approx 20 \text{ A/W}$  and  $g \approx 1000$ , as discussed in detail later.

## V. ANALYSIS AND DISCUSSION

### A. Extraction of the QWIP dynamic parameters

We now focus on interpretation of the experimental results. We assigned the PC peaks of the two QWIP structures occurring at  $\sim 1.42 \mu\text{m}$ , shown in Fig. 2(a) and 2(c), to the ISB transitions from the QW's bound state  $E_{1-}$  to the resonant  $E_{+}$  states in the continuum. These transition energies were confirmed, within the experimental error, by the 10-band  $k \cdot p$  model ( $1.48 \mu\text{m}$ ,  $0.84 \text{ eV}$ ), as shown in Fig. 1(b). As expected, these transitions were not dependent on the barrier height, because the position of the  $E_{+}$  energy level was related to the N content in the (Ga,In)(As,N) layer, which was the same in both samples (neglecting the small effect of the barrier height on  $E_{1-}$ ).

The absorption minimum occurring at  $\sim 1.42 \mu\text{m}$  in the normal incident transmission spectrum in Fig. 3(a), and the absence of a PC peak at  $1.42 \mu\text{m}$  from the (Ga,In)As QW reference sample strengthen our interpretation. Taking into account the losses in the optical path, the size of the detector, and the coupling efficiency of the light, we found that the RT peak current responsivity was  $\sim 18$  and  $21 \text{ A/W}$  for the (Ga,In)(As,N)/(Ga,As) and (Ga,In)(As,N)/(Al,Ga)As QWIPs, respectively. As we demonstrate later, the very high responsivity of the two QWIPs was related to the long lifetime of the excited states and the small emission probability to the 3D continuum. We ascribed the reduction in the PC signal intensity as a function of temperature in the (Ga,In)(As,N)/(Ga,As) QWIP as arising from the thermal emission of free carriers, i.e., electrons, out of the (Ga,In)(As,N) QWs. The near-equal but opposite sign ( $\pm 50 \text{ meV}$ ) of the activation energy of the decreased PC signal [Fig. 2(b)] and the increased dark current signal [Fig. 3(c)] confirmed this assumption. The exponential increase in the PC intensity as a function of temperature of the (Al,Ga)As barrier QWIP can be explained by the temperature dependence of the escape probability of excited electrons from the localized  $E_{+}$  resonant level into the 3D continuum.

We used standard QWIP theory<sup>20</sup> to extract the parameters that controlled the high responsivity of the QWIPs structures

in this work. The relaxation dynamics of the excited carriers were studied using LO phonon scattering theory.<sup>21,22</sup>

In general, the spectral responsivity is given by  $R_i = (q/h\nu)\eta g_{\text{photo}}$ , where  $\nu$  is the photon frequency,  $\eta$  is the absorption quantum efficiency, and  $g_{\text{photo}}$  is the gain. Taking into account that  $R_i = 18$  and  $21$  A/W at  $\lambda = 1.42$   $\mu\text{m}$ , and that the measured value of  $\eta$  was  $0.015$  [Figs. 2(a), 2(c), and 3(a)], we calculated the gain at RT to be  $g_{\text{photo}} = 10482$  and  $1222$  for the (Ga,As) and (Al,Ga)As QWIPs, respectively, assuming the same absorption occurred for both structures. Under a typical approximation,  $g_{\text{photo}} = p_e/Np_c$  and  $p_c \approx t_{\text{transit}}/\tau_c$ , where  $p_e$  is the escape probability from an excited state,  $N$  is the number of wells in the structure,  $p_c$  is the capture probability into the well of an excited electron,  $\tau_c$  is the capture time of an excited electron into the well, and  $t_{\text{transit}}$  is the transit time across a single QW region, including surrounding barriers. Usually,  $p_e$  is taken to be unity if the excited state is in the continuum above a well.<sup>20</sup>

Because the barrier height of the (Al,Ga)As QWIP was  $200$  meV higher than the (Ga,As) barrier, the electron thermal escape probability (i.e., the dark current) from the QW was lower, and the dominant factor that influenced the exponential increase in the PC signal with temperature in this structure [Fig. 2(c) and 2(d)] was related to the escape probability of the electrons from the excited quasibound state,  $E_+$ , as discussed later.

Our interpretation regarding the thermal escape of the QW's confined electrons from the (Al,Ga)As barrier QWIP was confirmed from the low dark current observed and the high activation energy of the dark current [Fig. 3(b) and 3(c)]. We extracted the excited electrons' escape probability  $p_e$  from the activation energy of the PC of the (Ga,In)(As,N)/(Al,Ga)As QWIP [ $E_a = 137$  meV, Fig. 2(d)] using a simple statistical expression:  $p_e = \exp(-E_a/kT) = 5.14 \times 10^{-3}$  (using Boltzmann statistics). In this calculation, we ignored the  $T^{3/2}$  weaker temperature dependence of the mobility and relied on the clear exponential dependence of the PC ( $\text{PC} \propto \eta \times g_{\text{photo}}$ , assuming that  $\eta$  is independent of temperature). From the relationship  $g_{\text{photo}} = p_e/Np_c$ , we extracted  $p_c = 4.2 \times 10^{-7}$  and the capture time as  $\tau_c \approx t_{\text{transit}}/p_c = 59$  ns, using an RT mobility of  $1000$   $\text{cm}^2/\text{V}\cdot\text{s}$  for the electrons above the (Al,Ga)As barriers. If we assume that the values of  $p_e$  and  $\eta$  are about the same for the (Ga,As) and (Al,Ga)As barrier structures and use the procedure described previously, our calculations gave  $p_c = 4.9 \times 10^{-7}$  and  $\tau_c = 120$  ns at RT, using an RT mobility of  $8500$   $\text{cm}^2/\text{V}\cdot\text{s}$  for the electrons in the (Ga,As) barrier, for the (Ga,In)(As,N)/(Ga,As) QWIP.

The values of the responsivity, gain, and excited carrier capture time are a few orders of magnitude higher than typical values for standard (Ga,As)/(Al,Ga)As QWIP structures. We suggest here, and demonstrate later, that slowing of the carrier relaxation time and decrease in the excited carrier emission probability are the result of the strongly modified band structure in (Ga,In)(As,N) and the N-localized resonant nature of the  $E_+$  level around  $k = 0$ , forming a BSIC.

### B. Application of LO phonon scattering theory to the excited carrier relaxation and escape time

We based our scattering analysis on the unique dispersion nature of the  $E_+$  level. From the BAC model, the wave function

$\psi_+$  can be described as a linear combination of the unperturbed 3D continuum  $\psi_{co}$  and the resonant N-localized  $\psi_N$  wave functions:

$$\psi_+ = \alpha_c \psi_{co} + \alpha_N \psi_N$$

where  $\alpha_c^2 + \alpha_N^2 = 1$ . The fractional N character,  $f_N = \alpha_N^2$ , of the  $E_+$  state provides a useful measure of how much the N-related states perturb the conduction band continuum wave functions. Figure 1(a) shows a drawing of the characteristic features of the conduction band dispersion calculated using the 10-band  $k \cdot p$  model for the (Ga,In)(As,N) layer studied in this work. An examination of the  $E_+$  dispersion curve shows that near  $k = 0$ , it has a near-unperturbed, localized  $\psi_N$  nature ( $\alpha_N^2 \approx 0.95$  at  $k = 0$ , Fig. 1(a) and 1(c)). As shown in Fig. 1(c) for  $k > k_0$  (the anticrossing point),  $E_+$  is tangential to the 3D continuum dispersion curve. Recently, experimental evidence for the dispersion curves of dilute nitrides was provided by Patane *et al.*<sup>23</sup> from magnetotransport data of (Al,Ga)As/Ga(As,N) resonant tunneling diodes. In their work, it was shown that the  $\Gamma$  character of the states was strongly reduced at the energy of the isolated N-impurity level. In addition, as the N content increases, the isolated N atoms, N–N pairs, and higher-order clusters tend to reduce the  $\Gamma$  character of the electronic states.

The conduction subband dispersion curves in the  $xy$  plane based on the BAC model are shown schematically in Fig. 6. The dashed (blue) lines denote the dispersions of the confined  $E_{1-}$  and  $E_{2-}$  subbands in the QW and the  $E_+$  band. The large-dot (blue) line denotes the above-barrier 3D continuum states of the (Ga,In)(As,N) layer. An electron that has been optically excited to the bottom of the  $E_+$  level at  $k = 0$  can be scattered into the (Ga,In)(As,N) continuum above-barrier states with different low or high  $k$ -wave vectors. In the case of scattering into a high  $k$ -wave vector state (emission scattering), the electron are attracted into the (Ga,As)—or (Al,Ga)As—continuum, above the barriers, by the external electric field, thus contributing to the PC. In the second case, the electron relaxes by LO phonon emission scattering into a low  $k$  vector continuum wave function state. From there, it can be scattered efficiently by acoustic or LO phonon emission into

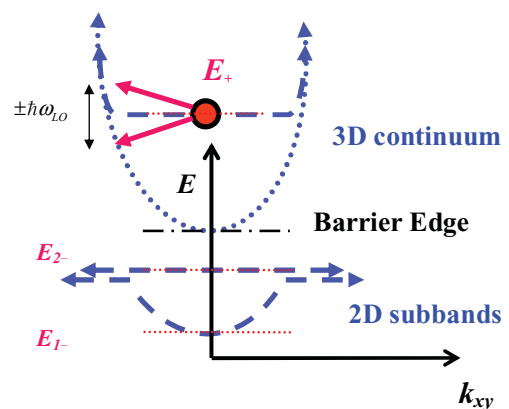


FIG. 6. (Color online) Schematic dispersion subband curves in the  $xy$  plane. The dashed (blue) lines denote the dispersion of the confined subbands  $E_{1-}$  and  $E_{2-}$  in the (Ga,In)(As,N) QW plane and the  $E_+$  band in the continuum. The large-dotted (blue) line denotes the above-barrier 3D continuum dispersion band.

the confined ground state  $E_{1-}$  in the well (capture scattering). Based on the relevant  $E_{1-}$  dispersion curve (shown in Fig. 6), the direct scattering from the  $E_+$  ( $k = 0$ ) state into the confined  $E_{1-}$  level by an LO phonon is not allowed from energy and momentum conservation considerations.

The following text provides details of the numerical estimation of the relaxation time  $\tau_R$  and an escape time  $\tau_e$  of the electron, excited to the  $E_+$  level. The dominant scattering mechanism between subbands separated by more than the optical phonon energy is the emission of the LO phonons. To compute the relaxation time  $\tau_R$  of an electron in the localized  $E_+$  level ( $k = 0$ ) to a final state  $\psi_f$ , we used the Fermi golden rule expression derived by Kinsler and Harrison for a two-dimensional (2D) carrier-distribution (see Ref. 22, page 296) as

$$\frac{1}{\tau_i} = \frac{\Gamma''}{2} \Theta \left( k_i^2 - \frac{2m^* \Delta}{\hbar^2} \right) \times \int_{-\infty}^{+\infty} \frac{\pi |G_{if}(K_z)|^2}{\sqrt{K_z^4 + 2K_z^2(2k_i^2 - \frac{2m^* \Delta}{\hbar^2}) + (\frac{2m^* \Delta}{\hbar^2})^2}} dK_z, \quad (1)$$

where

$$\Gamma'' = \frac{2m^* e^2 \omega_{LO}}{(2\pi)^2 \hbar^2} \left( \frac{1}{\varepsilon_\infty} - \frac{1}{\varepsilon_s} \right) \left( N_0 + \frac{1}{2} \pm \frac{1}{2} \right) \quad (2)$$

and  $m^*$  is the effective electron mass,  $e$  is the electron charge,  $\omega_{LO}$  is the LO phonon frequency, and  $\varepsilon_\infty$  and  $\varepsilon_s$  are the high- and low-frequency permittivities of the material, respectively. The factor  $(N_0 + \frac{1}{2} \pm \frac{1}{2})$  denotes the phonon density within the crystal. The upper signal preceded by the  $\pm$  term denotes the phonon emission and the lower phonon absorption, respectively. The phonon absorption process was ignored in our calculations, because it is slower than the phonon emission process, even at RT (e.g., four times slower at RT).<sup>22</sup> The Heaviside function  $\Theta$  was required for energy conservation, where  $\Delta = E_f - E_i \pm \hbar\omega_{LO}$  and  $E_i$  and  $E_f$  are the initial and final subband edge states, respectively. The term  $K_z$  is the phonon momentum in the growth direction, and  $k_i$  is the in-plane momentum of the carriers in the initial state. We assumed that  $k_i = 0$  for a BSIC in the  $E_+$  subband.

The form factor  $G_{if}(K_z)$  is given by

$$G_{if}(K_z) = \int \psi_f^*(z) e^{-iK_z z} \psi_i(z) dz, \quad (3)$$

where  $\psi_i$  and  $\psi_f$  are the electron envelope wave functions of the final and initial states, respectively. In a conventional 2D QW system, where  $\psi_i$  and  $\psi_f$  are the confined envelope wave functions, the form factor  $|G_{if}(K_z)|^2$  has a value close to unity:  $\sim 0.5$  for a 100-Å (Ga,As) infinitely deep QW.<sup>22</sup> In this work, the initial excited state  $\psi_i$  at  $E_+$  ( $k = 0$ ) was different from the conventional envelope function of an excited state in a QW. Taking into account the “nitrogen nature” of the dispersion curve of  $E_+$  at  $k = 0$ , we used a Gaussian-shaped wave function in our calculations [Eq. (4)] for the initial excited electron state  $\psi_i$  localized over a length  $b$ , describing an electron bound to a nitrogen center. As shown later, the highly localized Gaussian shape of  $\psi_i$  strongly influences the scattering processes. Following Kent and Zunger,<sup>15</sup> the localization length was taken to be  $b = 6$  Å. The most effective position of the nitrogen center, with respect to the final state,

was chosen for our calculations. As an example, the spatially slow-mode final state  $\psi_f$  was taken to be the lowest  $k$  vector 3D continuum state at the QW barrier edge normalized over a length  $L$  [Eq. (5)]. In our calculations, the normalization length was taken to be two QWIP periods; that is,  $L = 780$  and  $960$  Å for the (Ga,In)(As,N)/(Al,Ga)As and (Ga,In)(As,N)/(Ga,As) QWIPs, respectively.

$$\psi_i = \psi_N = \left( \frac{2}{\pi b^2} \right)^{1/4} \exp \left( \frac{-(z - z_0)^2}{b^2} \right) \quad (4)$$

$$\psi_f = \psi_{\text{continuum}} = \sqrt{\frac{2}{L}} \sin(K_z z) \quad (5)$$

We used  $m^* = 0.055m_0$  (related to the  $\psi_f$  density of states<sup>22</sup>) to describe the (Ga,In)As unperturbed 3D continuum dispersion curve, assuming a parabolic approximation. The (Ga,As) dielectric permittivities at infinite and zero frequency were taken to be 10.98 and 13.18, respectively, and the energy of the optical phonons was taken to be  $\hbar\omega_{LO} = 36$  meV. The result of the phonon emission scattering time calculations for the electron relaxation time  $\tau_R$  as a function of the position of the  $E_+$  energy at  $k = 0$  above the (Al,Ga)As barrier is shown in Fig. 7(a). The squared form factor for these calculations is shown in Fig. 7(b), showing a maximum value of  $1.6 \times 10^{-5}$ , which is four orders of magnitude smaller than that of standard ISB transition values<sup>22</sup> and reflects the difference between the dilute nitride-based structure and a conventional QWIP. For the position of  $E_+$  in this work ( $E_+ = 2.044$  eV), our calculations resulted in  $\tau_R = 38$  ns for the (Ga,In)(As,N)/(Al,Ga)As QWIP and  $\tau_R = 80$  ns for the (Ga,In)(As,N)/(Ga,As) QWIP. These results are of the same order of magnitude as the capture times extracted from the experimental results,  $\tau_c = 59$  ns for the (Ga,In)(As,N)/(Al,Ga)As QWIP and  $\tau_c = 120$  ns for the (Ga,In)(As,N)/(Ga,As) QWIP. We assigned the relatively long capture time  $\tau_c$  into the QWs to the slow relaxation mechanism of the excited electrons from the localized  $E_+$  level. This inefficient scattering mechanism acts as a bottleneck for the faster capture process of the low-energy electrons in the continuum above the QWs. The experimental results are consistent with the theoretical dependence of the scattering time on  $L$ , the QWIP period length [Eq. (5)].

We used the same procedure described previously to evaluate the escape time  $\tau_e$  of the localized electrons from the excited state  $E_+$  ( $k = 0$ ) into a spatially fast free-state mode (giving the minimal escape time)  $\psi_f$  in the 3D continuum. For these calculations, we used a higher  $k$  value above the anticrossing point  $k_0$ , calculated using Eq. (6):

$$E_{C_{\min}}^{(\text{Al,Ga})\text{As}} + \frac{\hbar^2}{2m^*} k^2 = E_+(k = 0). \quad (6)$$

The dependence of the electron escape time on the  $E_+$  energy is shown in Fig. 7(c). The squared form factor for these calculations is shown in Fig. 7(d), showing a maximum value of  $8.4 \times 10^{-3}$ . This form factor is two orders of magnitude larger than the one calculated previously [Fig. 7(b)] for scattering to the low  $k$  continuum state, reflecting a faster scattering rate. For  $E_+ = 2.044$  eV, above the valence band edge of (Ga,As), the calculated escape time (to the  $k > k_0$  state) was  $\tau_e = 88$  ps for the (Ga,In)(As,N)/(Al,Ga)As QWIP. Taking

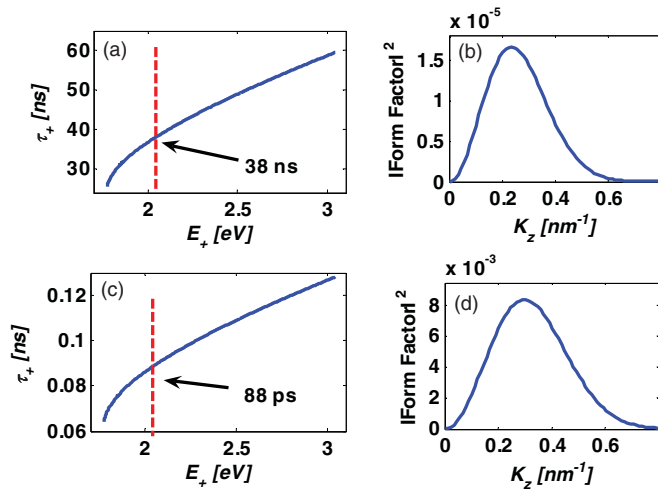


FIG. 7. (Color online) (a) The scattering time via LO phonon emission for an electron initially at  $E_+$  ( $k = 0$ ) and finally in the spatially slow-mode (low  $k$ ) continuum state as a function of the position of the  $E_+$  energy above the (Al,Ga)As barrier. (b) The squared form factor  $|G_{if}(K_z)|^2$ . (c) The scattering time via LO phonon emission for an electron initially at  $E_+$  at  $k = 0$  and finally in the spatially fast-mode continuum ( $k > k_0$ ) state as a function of the position of the  $E_+$  energy above the (Al,Ga)As barrier. (d) The square of its form factor. The valence band edge of (Ga,As) before spin-orbit split-off and any strain effect was chosen as the energy reference level for  $E_+$ .

into account the localized nature of the excited electrons at  $E_+$  ( $k = 0$ ), we used an “attempt frequency” approach,  $\tau_e = \frac{h}{kT} \exp(\frac{E_a}{kT})$ , to estimate the electron escape time into the continuum from the  $E_+$  exited level. Using the experimental escape probability,  $p_e = \exp(-E_a/kT) = 5.14 \times 10^{-3}$ , resulted in a value of  $\tau_e = 30$  ps, which is slightly faster than the calculated value of 88 ps when applying LO scattering theory. The dependence of the scattering equation [Eq. (1)] on the phonon density explains the exponential increase in the PC with temperature for the (Ga,In)(As,N)/(Al,Ga)As QWIP. The PC activation energy of the (Ga,In)(As,N)/(Al,Ga)As QWIP is explained by the difference in energy between the bound state at  $E_+$  ( $k = 0$ ) and the 3D continuum state at  $k > k_0$  [Fig. 1(c)].

### C. Bound-state coupling to the continuum extended states

The basic characteristic of BSICs in the absence of a scattering mechanism, such as LO phonons, is an infinite lifetime.

The negligible experimental escape rate ( $1/\tau_e = 1/30$  ps), compared to characteristic tunneling rate to continuum from excited quasi-bound state in standard QWIP, reflects the inefficient tunneling process, for electrons, from the localized excited state at  $E_+$  ( $k = 0$ ) to the 3D continuum. In addition, as shown in Fig. 5, the measured PC dependence on the bias voltage shows that an applied electric field does not affect the emission probability, and the linear relationship is attributed exclusively to the field dependence of the barrier electron transition time  $t_{\text{transit}}$ . These results confirm the low coupling strength between the localized state at  $E_+$  ( $k = 0$ ) and the 3D continuum. In addition, they show the dominant effect of phonon scattering on emission probability compared with tunneling, as reflected in the increase in the PC signal intensity as a function of temperature for the (Ga,In)(As,N)/(Al,Ga)As QWIP.

## VI. CONCLUSIONS

The overall close agreement between the experimental results and our model demonstrates that the measured QWIPs’ high gain and responsivity values represent unique transitions from the bound states in a QW to a BSIC. This excited state is characterized by a relatively long relaxation lifetime and a temperature-dependent escape probability. In addition, the excited state energy lies above the QW potential barrier, and the quantum mechanical coupling of the excited state with the surrounding continuum is insignificant. As a result, in the absence of thermal scattering mechanism, this state should have an infinite lifetime. This work experimentally illustrates BSICs formed from highly localized resonances of nitrogen isoelectronic doping centers, which decoupled from the continuum by anticrossing interaction. Our results also demonstrate a new type of QWIP detector that has a new degree of freedom for the design of its electronic properties.<sup>24</sup> A comprehensive and detailed understanding of how the unusual and unique conduction band of (Ga,In)(As,N) can modify the optical and transport properties of heterostructure systems of this material remains a challenge.

## ACKNOWLEDGMENTS

We thank N. Moiseyev<sup>7</sup> and O. Cohen, of the Technion-Israel, for fruitful discussions. This work was supported in part by the Technion-Russell-Berrie Nanotechnology Institute under Grant No. 2009101.

\*asafalbo@gmail.com

<sup>1</sup>J. von Neumann and E. Wigner, *Z. Phys.* **30**, 465 (1929).

<sup>2</sup>N. Moiseyev, *Phys. Rev. Lett.* **102**, 167404 (2009).

<sup>3</sup>H. Friedrich and D. Wintgen, *Phys. Rev. A* **32**, 3231 (1985).

<sup>4</sup>J. Okolowicz, M. Ploszajczak, and I. Rotter, *Phys. Rep.* **374**, 271 (2003).

<sup>5</sup>D. R. Herrick, *Phys. B* **85**, 44 (1977).

<sup>6</sup>F. H. Stillinger, *Phys. B* **85**, 270 (1977).

<sup>7</sup>F. Capasso, C. Sirtori, J. Faist, D. L. Sivco, S.-N. G. Chu, and A. Y. Cho, *Nature (London)* **358**, 565 (1992).

<sup>8</sup>J. Salzman, G. Lenz, E. Baruch, and E. Finkman, *Appl. Phys. Lett.* **59**, 1858 (1991).

<sup>9</sup>G. Bastard, U. O. Ziemelis, C. Delalande, and M. Voos, *Solid State Comm.* **49**, 671 (1984).

<sup>10</sup>Y. Plotnik, O. Peleg, F. Dreisow, M. Heinrich, S. Nolte, A. Szameit, and M. Segev, *Phys. Rev. Lett.* **107**, 183901 (2011).

- <sup>11</sup>M. Henini, *Dilute Nitride Semiconductors* (Elsevier, Oxford, 2005).
- <sup>12</sup>W. Shan, W. Walukiewicz, J. W. Ager, E. E. Haller, J. F. Geisz, D. J. Friedman, J. M. Olson, and S. R. Kurtz, *Phys. Rev. Lett.* **82**, 1221 (1999).
- <sup>13</sup>E. P. O'Reilly, A. Lindsay, P. J. Klar, A. Polimeni, and M. Capizzi, *Semicond. Sci. Technol.* **24**, 033001 (2009).
- <sup>14</sup>E. P. O'Reilly, A. Lindsay, S. Tomic, and M. Kamal-Saadi, *Semicond. Sci. Technol.* **17**, 870 (2002).
- <sup>15</sup>P. R. C. Kent and A. Zunger, *Phys. Rev. B* **64**, 115208 (2001).
- <sup>16</sup>A. Albo, C. Cytermann, G. Bahir, and D. Fekete, *Appl. Phys. Lett.* **96**, 141102 (2010).
- <sup>17</sup>A. Albo, A. Vardi, D. Fekete, and G. Bahir, *Appl. Phys. Lett.* **94**, 093503 (2009).
- <sup>18</sup>A. Albo, D. Fekete, and G. Bahir, *Phys. Status Solidi C* **5**, 2323 (2008).
- <sup>19</sup>S. T. Ng, W. J. Fan, Y. X. Dang, and S. F. Yoon, *Phys. Rev. B* **72**, 115341 (2005).
- <sup>20</sup>H. Schneider and H. C. Liu, *Quantum Well Infrared Photodetectors, Physics and Applications* (Springer, Berlin, 2007).
- <sup>21</sup>R. Ferreira and G. Bastard, *Phys. Rev. B* **40**, 1074 (1989).
- <sup>22</sup>P. Harrison, *Quantum Wells, Wires and Dots, Theoretical and Computational Physics of Semiconductors and Nanostructure*, 2nd ed. (Wiley, Chichester, West Sussex, UK, 2007).
- <sup>23</sup>A. Patane, J. Endicott, J. Ibanez, P. N. Brunkov, L. Eaves, S. B. Healy, A. Lindsay, E. P. O'Reilly, and M. Hopkinson, *Phys. Rev. B* **71**, 195307 (2005).
- <sup>24</sup>A. Albo, D. Fekete, and G. Bahir, US Patent Application 2011/0133088A1.